



Effect of Specimen Thickness on the Fracture Toughness of a NiTi Shape Memory Alloy

B. Abut¹ · B. Haghgouyan² · I. Karaman¹ · D. C. Lagoudas^{1,2}

Received: 1 December 2020 / Revised: 31 December 2020 / Accepted: 21 January 2021 / Published online: 9 April 2021
© ASM International 2021

Abstract In this study, the thickness dependence of the fracture toughness in a NiTi shape memory alloy (SMA) is investigated. To this aim, compact tension specimens with various thicknesses were tested at room temperature, while in fully martensitic state, and under mode-I loading. Stable crack growth was observed in all specimens, regardless of the thickness. The resistance curves were obtained from load–displacement data and the J -integral values were determined using a recently proposed methodology for SMAs. Critical J values were obtained and compared to reveal the thickness dependence of the fracture toughness. Strains were measured using digital image correlation technique to evaluate the nonlinear deformation zone near the crack tip. To investigate the fracture mechanism, the fracture surface analysis was carried out. The results suggest modifications towards relaxing the existing thickness requirements for fracture toughness measurements in SMAs.

Keywords Fracture toughness · Crack growth · Thickness effect · NiTi shape memory alloy

Introduction

Shape Memory Alloys (SMAs) are a unique class of active materials with the ability to repeatedly undergo and recover large deformation when subjected to thermomechanical inputs [1]. This ability has roots in a displacive phase transformation between austenite (the parent phase) and martensite phase (the product phase) [2]. SMAs such as NiTi have been studied in the last few decades due to their widespread application in biomedical industry [3, 4]. More recently, they have been of interest as solid-state actuators in aerospace industry where high actuation energy density alongside reduction in weight, volume and complexity is desired [5–7]. In such applications, repeatable phase transformation in the presence of high stresses can result in crack initiation and propagation [8]. Therefore, successful applications of SMAs under various thermomechanical loading paths requires a complete understanding of their fracture behavior, and accurate measurement of fracture parameters [9]. The thermo-mechanical behavior of SMAs has been widely explored and few ASTM standards has been recently established for their uniaxial characterization (e.g. Refs. [10, 11]). However, there is limited knowledge about the fracture behavior of SMAs and there are no specific standards available for measuring their fracture parameters, other than ASTM standards related to fracture mechanics for conventional materials.

One of the most important criteria for the analysis and design of SMAs, especially for actuation applications, is the fracture toughness. Fracture toughness of NiTi SMAs have been reported in few papers [12–21] and the effect of various material and testing parameters on the fracture response of NiTi have been experimentally investigated. The effects of temperature on fracture toughness of NiTi SMAs have been investigated in few studies. Holtz et al.

This article is part of a special topical focus in *Shape Memory and Superelasticity* on the Mechanics and Physics of Active Materials and Systems. This issue was organized by Dr. Theocharis Baxevanis, University of Houston; Dr. Dimitris Lagoudas, Texas A&M University; and Dr. Ibrahim Karaman, Texas A&M University.

✉ D. C. Lagoudas
lagoudas@tamu.edu

¹ Department of Materials Science and Engineering, Texas A&M University, College Station, TX 77843, USA

² Department of Aerospace Engineering, Texas A&M University, College Station, TX 77843, USA

[12] and Maletta et al. [19] reported a monotonic increase in fracture toughness with temperature. Gollerthan et al. [16], showed that the fracture toughness of NiTi was very close for fully martensitic and transforming materials (31 and 34 MPa $\sqrt{\text{m}}$, respectively) while that of stable austenite was substantially higher (53 MPa $\sqrt{\text{m}}$). Daly et al. [14] investigated fracture properties of thin (160- μm -thick) edge-cracked NiTi specimens. They performed tests on specimens with different crack sizes and used the maximum load to calculate fracture toughness using Linear Elastic Fracture Mechanics (LEFM). An average fracture toughness (K_c) of ~ 51 MPa $\sqrt{\text{m}}$ was reported. They found that the results were independent of crack size to width (a/W) ratio in the range $0.42 < a/W < 0.55$. Ahadi et al. [22] studied the grain size dependence of fracture toughness and crack growth resistance in NiTi. They obtained critical stress intensity factors for compact tension (CT) specimens with grain sizes in the range of 10 to 1500 nm. They reported a transition from rising to flat R -curve behavior, a monotonic decrease in the size of crack-tip transformation zone, and fracture toughness changing from ~ 46 to ~ 25 MPa $\sqrt{\text{m}}$ with grain size reduction. They attributed this behavior to the grain size dependence of transformation stress and crack propagation path. Katanchi et al. [18] studied mixed-mode fracture of NiTi and performed fracture experiment using butterfly-shaped specimens to obtain fracture toughness in the range of mode-I to mode-II by changing the loading angle. They calculated stress intensity factors using LEFM formulation and found that the material was tougher in mode-I loading compared with mode-II loading conditions as the size of the transformed zone decreased and the fracture surface roughness increased. Mutlu et al. [20] studied the effect of loading rate on fracture toughness of NiTi under mode-I loading. They tested 1-mm thick CT specimens at different quasi-static-range loading rates and calculated critical stress intensity factors. Interestingly, an increasing–decreasing trend was reported with increasing loading rate while the transformation zone near the crack tip was found to be decreasing because of the increase in near-tip temperature at higher loading rates.

Majority of the published studies in the literature on fracture of NiTi SMAs are based on LEFM approach and use the ASTM E399 standard [23]. Most of the studies, however, do not comply with the small-scale yielding condition, required for validity of LEFM. There have also been efforts [17, 19, 20] to measure the fracture toughness using displacement data, obtained from digital image correlation (DIC). Unlike the standard test methods, this method requires relatively sophisticated testing setup and rigorous post processing. In general, because of the complex fracture mechanics associated with martensitic transformation/reorientation, applying the existing fracture

mechanics theories and standard test methods/requirements to SMAs is not straightforward [24]. To address some of these challenges, a method is proposed by Haghgouyan et al. [25] that uses the J -integral, introduced by Rice [26], as the fracture criterion for measuring the fracture toughness of SMAs. This method is based on the Elastic Plastic Fracture Mechanics (EPFM) and modifies the existing ASTM E-1820 [27] standard to take into account the martensitic transformation/reorientation-induced changes in the elastic properties of SMAs.

Reviewing the literature, the reported fracture toughness values have been measured using specimens with different thicknesses, however, each study has considered a specific value of thickness. In other words, there is no data available from the same material system and testing conditions, but with different thickness values. In conventional metals, it is well-established that the fracture toughness values tend to decrease with specimen thickness until a plateau is reached in the toughness-thickness trend, after which the fracture toughness becomes relatively insensitive to thickness [28]. This apparent asymptote is referred to as the *plane-strain fracture toughness*, a size-independent material property. Attributing this behavior to a transition from *plane stress* to *plane strain*, however, is too simplistic since there is always some level of stress triaxiality along the crack front. Moreover, as mentioned earlier, the fracture behavior of SMAs is rather complex compared to the conventional metals and extra caution should be taken when applying the existing fracture mechanics theories to them. Therefore, the thickness requirements developed for conventional metals to ensure a constraint-independent value of fracture toughness may not necessarily apply to SMAs, and a comprehensive set of experiments on specimens with various thicknesses is required for a rigorous evaluation.

The present study is the first investigation, to the best of our knowledge, into the effect of specimen thickness on the fracture toughness of NiTi SMAs. The fracture toughness values are determined using CT specimens with four different thicknesses. Full-field strain measurements and fracture surface analysis are carried out to investigate the extent of near-tip nonlinear deformation zones and reveal the underlying fracture mechanisms. The remainder of the paper is structured as follows. In the next section, material characterization and experimental procedures are provided. Then, the results are presented and discussed. Finally, the paper is concluded with a summary of key findings.

Experimental Procedures

Material

For this study, Ni_{49.5}Ti_{50.5} (at.%) was acquired from ATI. The material was fabricated using the Vacuum Induction Melting/Vacuum Arc Melting (VIM/VAR) and processed via rotary forging at 800 °C followed by air cooling. For the sake of brevity, the material will be referred to as NiTi in what follows. A TA Q2000 differential scanning calorimetry (DSC) instrument was used to determine the transformation temperatures. A heat/cool cycle between 0 and 150 °C was performed at a rate of 10 °C/min. The corresponding DSC curve is plotted in Fig. 1a, from which the phase transformation temperatures were found using tangent lines as $M_s = 68$ °C, $M_f = 42$ °C, $A_s = 77$ °C, and $A_f = 106$ °C, where M_s , M_f , A_s , and A_f denote martensite start, martensite finish, austenite start and austenite finish temperatures, respectively.

Tensile Property Characterization

Tensile property characterization was performed on a servo-hydraulic MTS test frame equipped with a 10 kN load cell and an MTS extensometer. A dog-bone specimen with gage length, width, and thickness of 8, 3, and 0.8 mm, respectively, was pulled to failure at room temperature with an engineering strain rate of $5 \times 10^{-4} \text{ s}^{-1}$. The resulting stress–strain curve is plotted in Fig. 1b. Because the testing temperature was below M_f , the material initially had self-accommodated martensite structure. Upon loading, the material was deformed predominantly elastically with a Young's modulus of ~ 67 GPa, which is comparable with previously reported values for martensitic NiTi [29–31]. At ~ 200 MPa, a stress plateau appeared as the reorientation of martensitic variants took place. After the stress plateau was completed (at $\sim 5\%$ strain) the stress–

strain curve slope increased again as the reoriented martensite was deformed predominantly elastically. Further loading resulted in martensite yield at around 500 MPa and 10% strain. The specimen failed at ~ 950 MPa after more than 40% elongation.

Fracture Toughness Experiments

CT specimens with four nominal thicknesses (2, 3, 4, and 5 mm) were cut using wire electrical discharge machining (EDM). The thickness range investigated in this work is of practical importance, especially in actuation applications for aerostructures [32, 33]. A total of 12 specimens were cut, i.e. 3 specimens for each thickness value, to examine the consistency of the results. Specimens are enumerated considering their thickness values: specimens 1, 2, 3 with 2 mm thickness, specimens 4, 5, 6 with 3 mm thickness, specimens 7, 8, 9 with 4 mm thickness, and specimens 10, 11, 12 with 5 mm thickness. The specimens were prepared by mechanical grinding down to 1000 grit to remove the residual stresses and surface roughness and to aid crack size measurements. It should be noted that after mechanical grinding, the thickness of the specimens was reduced by ~ 0.15 mm. The geometry of the CT specimen is given in Fig. 2a where W , a_0 , and B are the specimen width, initial crack size, and thickness, respectively. A set of NiTi CT specimens with the selected thickness values are shown in Fig. 2b. Prior to the fracture experiments, fatigue pre-cracking was performed at room temperature under a constant load ratio of $R = P_{\min}/P_{\max} = 0.1$ and at a frequency of 10 Hz. The maximum load values used for pre-cracking were 800, 1200, 1600, and 2000 N for 2, 3, 4, and 5 mm thick specimens, respectively. Fatigue pre-cracking produced initial crack size to width ratio of $0.46 < a_0/W < 0.5$ for all specimens, which was in the range recommended by ASTM E1820. The specimen numbering

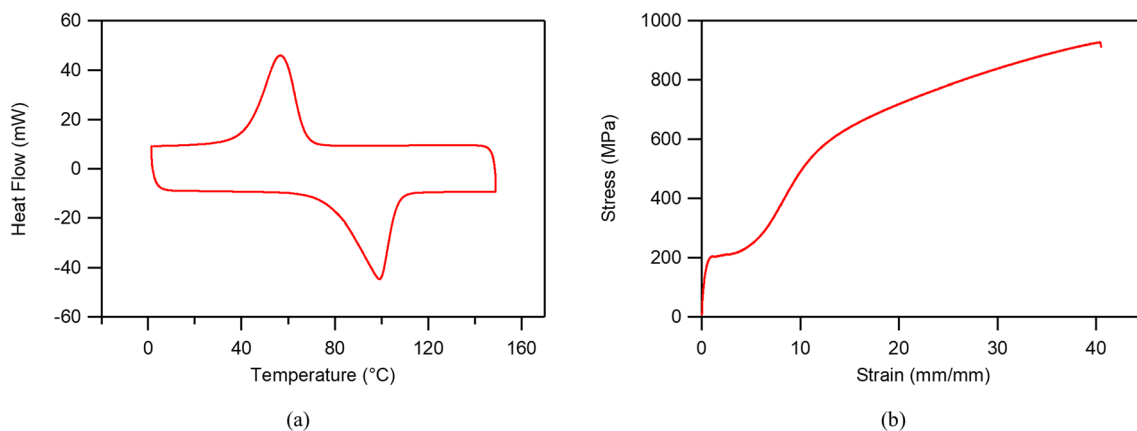


Fig. 1 Material characterization results for NiTi: **a** differential scanning calorimetry curve, **b** tensile stress–strain curve at room temperature

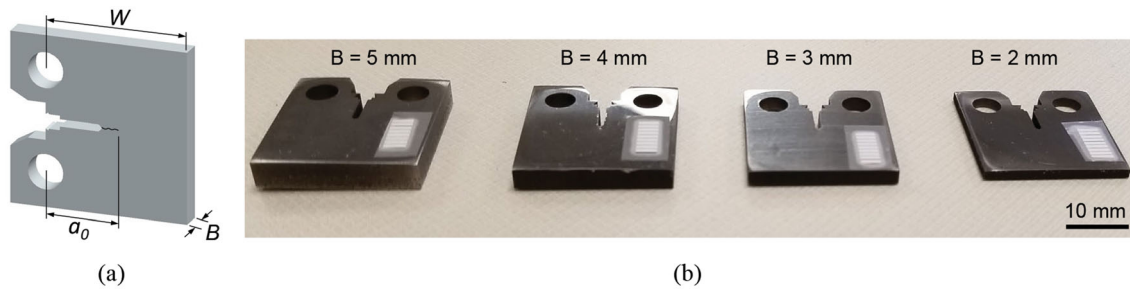


Fig. 2 **a** Schematic of a compact tension specimen where W , a_0 , and B are the specimen width, initial crack size, and thickness, respectively, **b** a set of NiTi compact tension specimens with $W = 20$ mm, $a_0 \approx 10$ mm and $B = 2, 3, 4,$ and 5 mm

Table 1 Specimen numbering and geometry for all tested compact tension specimens

Nominal thickness	Specimen #	B (mm)	a_0 (mm)
2 mm	Specimen 1	1.85	9.16
	Specimen 2	1.84	9.91
	Specimen 3	1.82	9.72
3 mm	Specimen 4	2.87	9.12
	Specimen 5	2.82	9.20
	Specimen 6	2.81	9.21
4 mm	Specimen 7	3.83	9.28
	Specimen 8	3.87	9.77
	Specimen 9	3.82	9.74
5 mm	Specimen 10	4.86	9.47
	Specimen 11	4.92	9.58
	Specimen 12	4.85	9.47

B is the thickness and a_0 is the initial crack size; the width is $W = 20$ mm in all specimens

and geometry for all tested CT specimens is provided in Table 1.

Mode-I fracture experiments were conducted at room temperature on an MTS-810 servo-hydraulic test machine under displacement control at a cross-head speed of 0.4 mm/min. Load and displacement were measured continuously during the tests using a 10 kN load cell and an MTS crack opening displacement (COD) gage, respectively. The use of COD gage allows for the direct measurement of displacement from the load line. For the sake of brevity, load line displacement will be referred to as displacement in what follows. Unloading/reloading sequences were carried out at 0.1 mm displacement changes to determine the specimen compliance, necessary to calculate J -integral and crack extension. The compliance values were corrected for rotation in accordance with the ASTM E1820.

DIC was used to measure in-plane strains near the crack-tip during the experiments. The use of DIC, an optical technique to measure full-field displacement, is preferred

over strain gages or extensometers due to the amount of information that can be collected during deformation history, and its ability to capture localized deformations. DIC has been emerged as a method to analyze deformation in SMAs [34–37] and evaluate the crack-tip parameters [38–40]. To this aim, surface of the specimens was uniformly sprayed with a thin layer of white paint, and then black speckles were sprayed to create the DIC pattern. Continuous recording of optical images was performed at 1 Hz by a Point Grey Grasshopper CCD camera equipped with a Tokina 100 mm f2.8 macro lens, resulting in an optical resolution of 0.02 mm/pixel. Postprocessing was performed via Vic2D-6 software (developed by Correlated Solutions) with a subset size of 21×21 pixel and a step size of 3 pixels.

Results and Discussion

Load–Displacement Data

The experimental load–displacement data for NiTi CT specimens tested at room temperature under mode-I loading are plotted in Fig. 3a–d for 2, 3, 4, and 5 mm specimens, respectively. As mentioned earlier, the unloading/reloading sequences were carried out throughout the experiments to determine the specimen compliance. The characteristics of the load–displacement curves were found to be very similar in all tested specimens, regardless of the thickness. The response was linear at the beginning of loading, associated with the elastic response of martensite. Upon further loading, a deviation from linearity was observed because of the reorientation of martensite at high stresses close to the crack tip. Further loading resulted in crack extension and the load–displacement curve reached its maximum load. After this point, upon further increase in the applied displacement, a gradual decrease in the load was observed. The load continued to decrease until the end of the experiment in absence of any major sudden load drop, indicating stable crack growth. The main difference

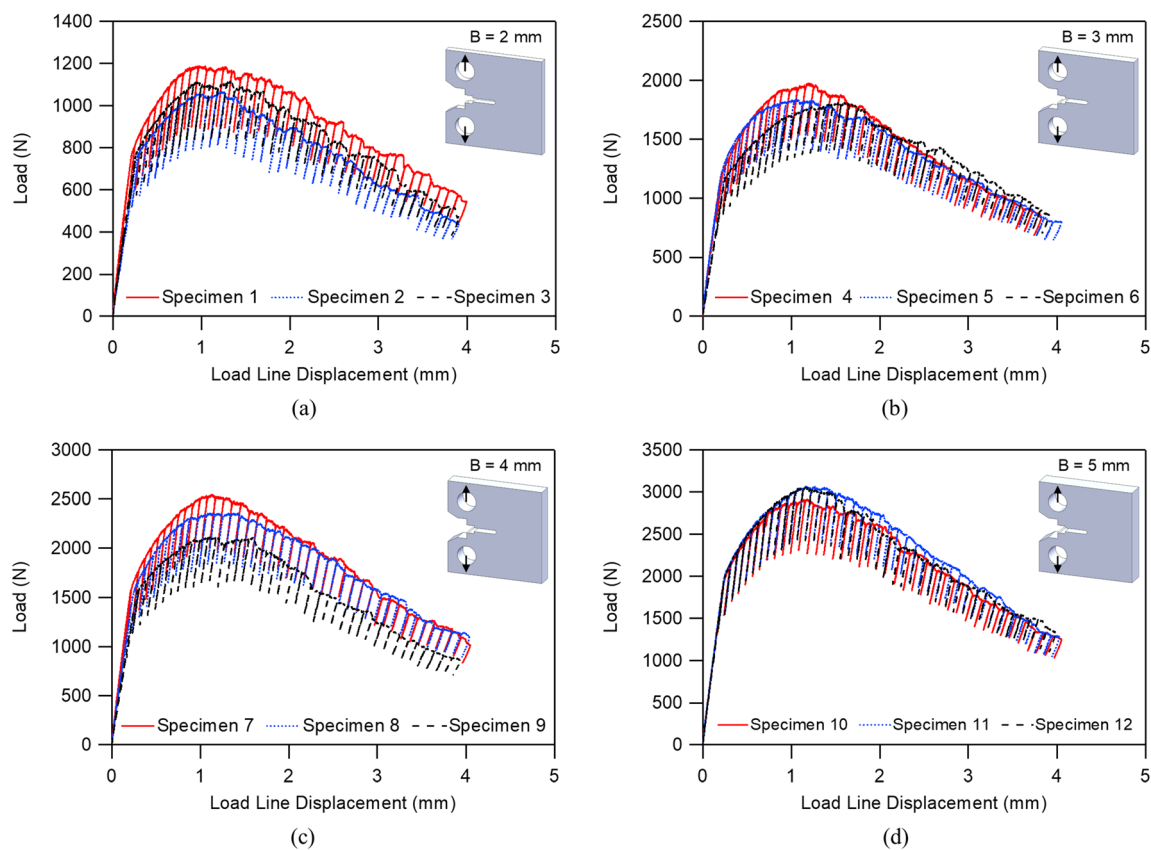


Fig. 3 Load–displacement curves for NiTi compact tension specimens with four different thickness values, **a** 2 mm, **b** 3 mm, **c** 4 mm, and **d** 5 mm, tested at room temperature in martensite under mode-I loading

in the load–displacement curves of specimens with different thicknesses was the maximum load that was reached during the experiments. For each thickness value, the small difference in the maximum load was because of the slightly different initial crack size and the sample to sample variation. The characteristic features of the load–displacement curves obviously do not comply with those of a linear elastic material, indicating that the data cannot be interpreted on the basis of LEFM.

Strain Field and Reorientation Zone

In-plane strains were measured using DIC for all tested specimens. To be brief, the results presented here are from a single specimen at each thickness value (specimens 1, 4, 7 and 10), and correspond to an applied displacement of 2 mm on the loading path and a crack extension of ~ 1.5 mm. The strains parallel to the crack plane (ϵ_{xx}), in the loading direction (ϵ_{yy}), and in-plane shear strains (ϵ_{xy}) are shown in Fig. 4a–c, respectively. It can be seen that the size and the shape of all the strain contours were very similar for all components and in all specimens, regardless of the thickness, suggesting no significant thickness effect on the near-tip mechanical fields. It should be noted,

however, because DIC is a surface measurement technique, the strain plots correspond to the surface of the specimens where the plane stress condition prevails. Therefore, extra caution is required in drawing a conclusion based on a surface measurement since it may not represent the possible through-the-thickness variations.

To estimate the nonlinear deformation zone near the crack tip, in this case martensite reorientation zone, the von Mises equivalent strain is calculated and plotted in Fig. 4d. Considering the stress–strain response of the material (Fig. 1b), the martensite reorientation is completed at $\sim 5\%$. Therefore, the color bar is adjusted such that the red color represents reoriented martensite. It can be seen that in all cases, the nonlinear zone is large compared to the characteristic dimensions of the specimen. Note that the red region approximates the fully reoriented zone, and reorientation process starts at as early as $\sim 0.5\%$ strain. Hence, the region that is undergoing reorientation, i.e. material points outside the red and engulfed by the dark blue color, is even larger in size, clearly indicating that LEFM cannot be implemented to interpret the data.

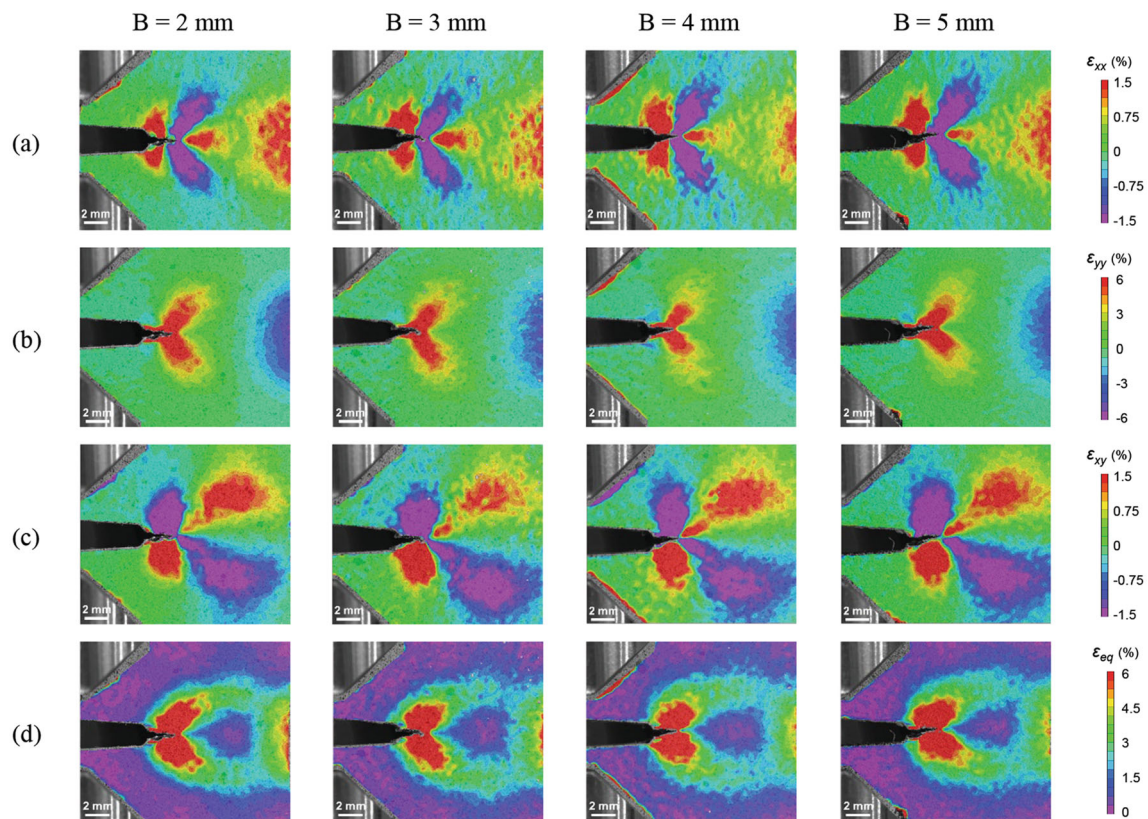


Fig. 4 Surface strain contours for NiTi compact tension specimens with 2, 3, 4, and 5 mm thicknesses (specimens 1, 4, 7, and 10, respectively) measured using digital image correlation. The plots

correspond to images taken at an applied displacement of 2 mm and after ~ 1.5 mm crack extension: **a** ϵ_{xx} , **b** ϵ_{yy} , **c** ϵ_{xy} , and **d** ϵ_{eq}

Resistance Curve and Fracture Toughness

To measure the resistance of the material to crack extension, fracture resistance curve (R -curve) was developed, which is essentially a plot of the fracture parameter, here selected as J due to the invalidity of LEFM for the present NiTi SMA, as a function of crack extension, Δa . To this end, for each loading increment on the load–displacement response corresponding to an unloading/reloading sequence, J and Δa values were obtained using the elastic compliance method. The method is described in the appendix. The ASTM E1820 procedure was followed to construct the J – R curves and obtain the fracture toughness near the onset of stable crack propagation (J_{Ic}). A construction line was drawn from the origin with a slope of $2\sigma_y$, where σ_y is the effective yield strength, defined here as the average of reorientation stress and the ultimate tensile strength (Fig. 1b). Two exclusion lines were drawn parallel to the construction line intersecting the abscissa at 0.15 and 1.5 mm following the ASTM standard. A power-law regression line was fit through the data confined by the exclusion lines. Finally, the critical J value was determined from the intersection of an offset line, drawn from $\Delta a = 0.2$ mm and parallel to the construction line, and the

regression line. The J – R curves for CT specimens with 2, 3, 4, and 5 mm thickness are plotted in Fig. 5a–d, respectively. Rising R -curve behavior was observed for all thickness values, associated with the reorientation of martensite near the crack-tip. As seen from the DIC results in Fig. 4d, the inelastic deformation zone at the crack tip was large compared to the characteristic dimensions of the CT specimen. The increase in the size of the inelastic zone during loading required the driving force to be increased to maintain the stable crack growth, resulting in the rising R -curve behavior.

The average J_{Ic} values for different thicknesses obtained from J – R curves are presented in Fig. 6a. Comparing the values from each thickness to the mean value obtained from all experiments, no specific trend was observed, suggesting no thickness effect on the fracture toughness of martensitic NiTi in the thickness range investigated in this work. The average extrapolated critical stress intensity factors, $K_{JIc} = \sqrt{J_{Ic} E_M}$, where E_M denotes the Young's modulus of martensite, are plotted together with LEFM-based critical stress intensity factors K_Q (if assumed to be valid) in Fig. 6b for comparison purposes. It can be seen that K_Q significantly underestimate the fracture toughness of NiTi as it is a load-based fracture parameter and doesn't

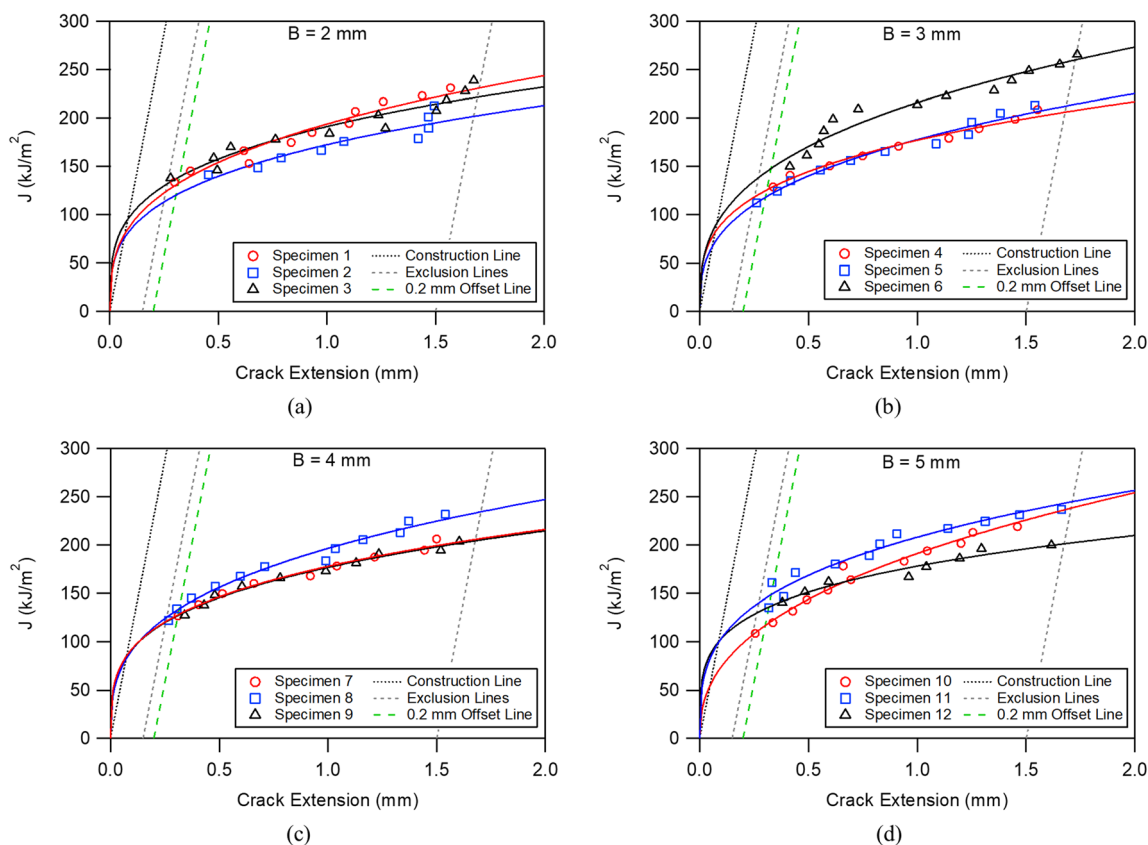


Fig. 5 J - R curves for NiTi compact tension specimens with four different thickness values, **a** 2 mm, **b** 3 mm, **c** 4 mm, and **d** 5 mm, tested at room temperature in martensite under mode-I loading

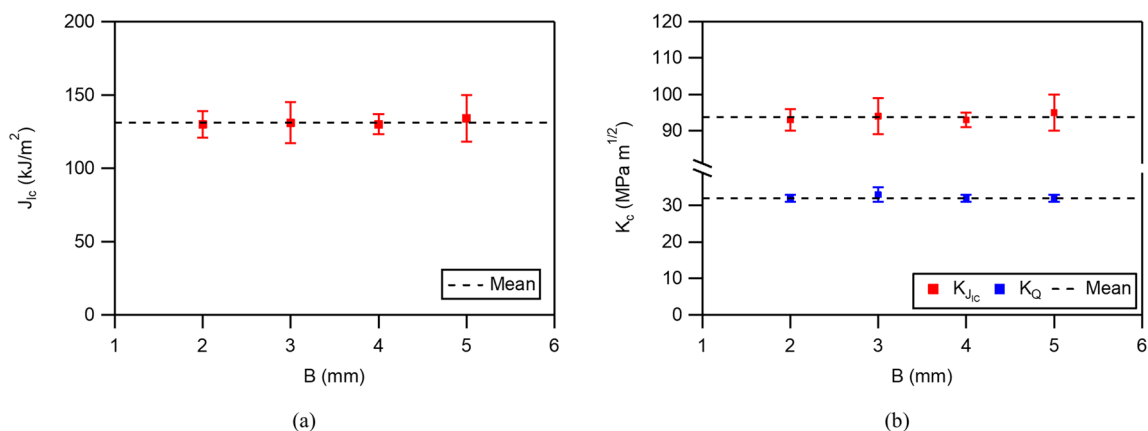


Fig. 6 Fracture toughness values for near equiatomic, martensitic NiTi shape memory alloy compact tension specimens with different thickness values: **a** J_{Ic} , **b** K_{Ic} and K_Q

account for the dissipation mainly caused by martensite reorientation. Nevertheless, similar to J_{Ic} (and therefore K_{Ic}) values, no thickness effect was observed by comparing K_Q values obtained from specimens with different thicknesses. The J_{Ic} , K_{Ic} and K_Q values are summarized in Table 2.

Fracture Mechanisms

The fracture surfaces were investigated with scanning electron microscopy (SEM). Figure 7 shows SEM images of the fracture surface of NiTi CT specimens with 3 mm and 5 mm thicknesses (specimens 4 and 10, respectively). According to the low-magnification images, no evidence of shear lip formation or crack tunneling were observed. The

Table 2 Average J_{Ic} , K_{JIc} and K_Q values for near equiatomic, martensitic NiTi shape memory alloy samples at different thickness values from 2 to 5 mm

B (mm)	J_{Ic} (kJ/m ²)	K_{JIc} (MPa m ^{1/2})	K_Q (MPa m ^{1/2})
2	130 ± 9	93 ± 3	32 ± 1
3	131 ± 15	94 ± 5	33 ± 2
4	130 ± 6	93 ± 2	32 ± 1
5	134 ± 16	95 ± 5	32 ± 1

flat fracture surfaces suggest much less sensitivity of the fracture toughness to the specimen thickness. The high-magnification images of the fracture surface reveal a quasi-cleavage fracture, i.e. dominated by cleavage exhibiting small parts with ductile tearing. The decrease in apparent toughness with specimen thickness is generally observed in materials that fail by ductile crack growth, i.e. their fracture mechanism is dominated by void nucleation, growth, and coalescence. In such materials, the crack extends preferably in areas that triaxiality is higher, resulting in a flat fracture surface in the middle, and shear lips near the edges. Therefore, in thicker specimens where the flat fracture surface dominates the thickness, the fracture toughness is not affected by the thickness. As observed here, the fracture mechanism of NiTi was dominated by

cleavage and the fracture surface was flat, explaining the insensitivity of fracture toughness to the specimen thickness.

Discussion on the Specimen Thickness Requirement for the Fracture Toughness of SMAs

According to the ASTM E1820 standard, the critical J value obtained from a J - R curve is a size-independent value of fracture toughness if b_0 , $B > 10 J_{Ic}/\sigma_Y$. The requirement for b_0 (the initial unbroken ligament) is to ensure J -dominance and the one for B is to ensure a constraint-independent value of fracture toughness. As mentioned earlier, σ_Y is the effective yield strength, and in conventional metals, it corresponds to the average of the ultimate tensile strength and the yield stress. In this work, σ_Y is interpreted as the average of stress required for initiation of reorientation and the ultimate tensile strength. Using yield stress instead of reorientation stress would underestimate the nonlinear deformation zone near the crack tip considerably. Implementing the properties obtained from the uniaxial stress–strain response (Fig. 1b) and the obtained critical J values (Fig. 6a), to satisfy thickness criterion the minimum required initial ligament and thickness is ~ 2.3 mm. While all the specimens meet the initial ligament requirement, the 2 mm-thick specimens

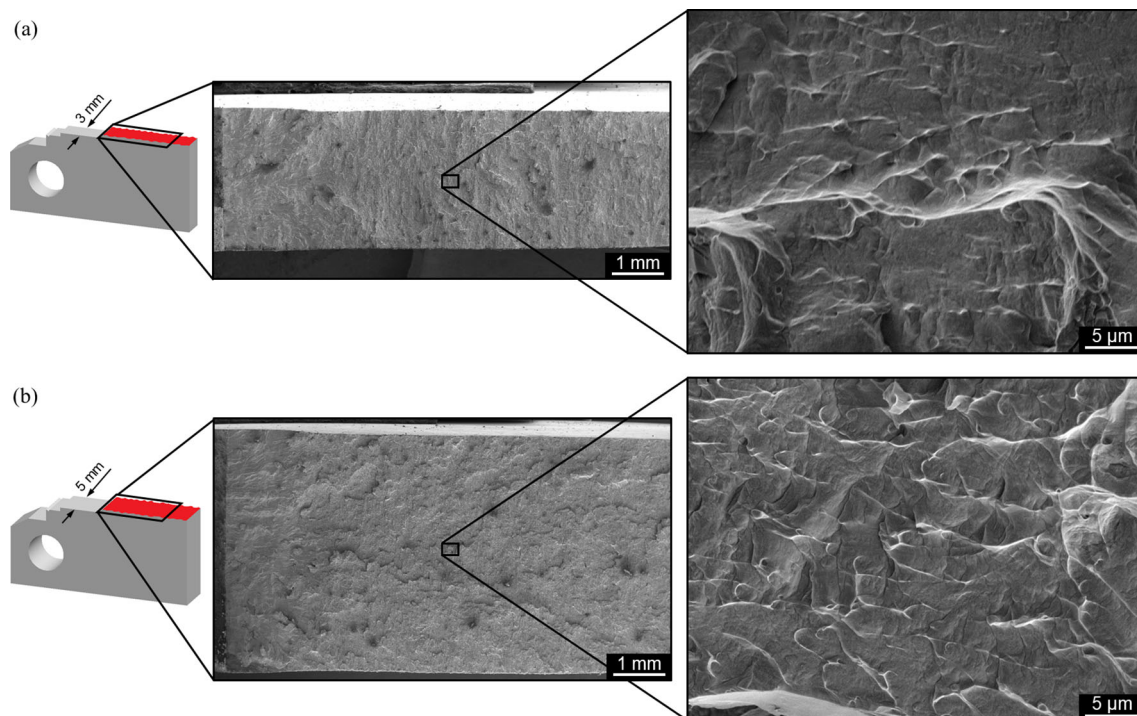


Fig. 7 SEM images showing the fracture surface of compact tension specimens with: **a** 3 mm thickness (Specimen 4), and **b** 5 mm thickness (Specimen 10). Low-magnification images show no

evidence of shear lips or crack tunneling while high-magnification images reveal a quasi-cleavage fracture mechanism

do not meet the thickness requirement. In general, for SMAs the yield stress should be interpreted as the stress required for either phase transformation, martensite reorientation, or austenite yield, depending on the ambient temperature.

Although NiTi SMAs show highly nonlinear response, they fail predominantly by cleavage fracture, and as observed from the SEM images in this study, crack tunneling and shear lips were not evident on the cleavage-dominated fracture surface. This is because the contribution of plastic deformation, responsible for a ductile fracture mechanism, on fracture of NiTi SMAs is smaller compared to the contribution from transformation/reorientation [41], and the size of the plastic zone at the crack tip is an order of magnitude smaller than the one anticipated in conventional elastic–plastic materials [42]. It is important to note that the material investigated in this study reached relatively high values of elongation to failure (more than 40%) and fracture toughness (95 MPa√m and above) compared to their counterparts such as NiTiHf [40], indicating that other SMAs are more likely to fail by cleavage fracture mechanism. This suggests that compared to conventional ductile metals, the fracture toughness in SMAs is less sensitive to the specimen thickness, and hence, the ASTM thickness requirement to ensure a constraint-independent fracture toughness measurement might be far stringent for SMAs, the deformation and fracture mechanism of which differs from those of conventional metals.

Summary and Conclusions

The effect of thickness on the fracture toughness of a near-equiatomic NiTi shape memory alloy was investigated while in fully martensitic state (below M_f). Mode-I fracture experiments were conducted at room temperature on compact tension specimens with four different thickness values (from 2 to 5 mm). Stable crack growth was observed in all tested specimens where the characteristics of the load–displacement curves were found to be very similar, regardless of the thickness. The in-plane strains, measured using digital image correlation, revealed relatively large zone of martensite reorientation as the main deformation mechanism acting near the crack tip. The resistance curves were developed using J -integral as the fracture parameter, and the fracture toughness values near the onset of stable crack propagation (J_{Ic}) were obtained. Comparing the J_{Ic} values showed no thickness effect for the thickness range investigated in this study. The insensitivity of fracture toughness to the specimen thickness is attributed to the underlying fracture mechanism in NiTi SMAs being dominated by cleavage resulting in a flat fracture surface with no shear lip formation. The results

obtained in this study can be extended to other NiTi-based SMAs, the fracture mechanism of which is similar to that of NiTi. Therefore, this work is considered a step towards modifying the existing thickness requirements for fracture toughness measurement in phase transforming materials.

Acknowledgements This material is based upon work supported by US Air Force Office of Scientific Research under Grant No. FA9550-18-1-0276, and by NASA University Leadership Initiative, under Grant No. NNX17AJ96A.

Appendix

Calculation of J -integral

J can be calculated at the i th unloading/reloading sequence as the sum of elastic and inelastic components

$$J_i = J_i^{el} + J_i^{in}, \quad (1)$$

where

$$J_i^{el} = \left[J_{i-1}^{el} + \frac{\eta_{i-1}^{el}}{Bb_{i-1}} A_{i-1,i}^{el} \right] \left[1 - \frac{\gamma_{i-1}^{el}}{b_{i-1}} (a_i - a_{i-1}) \right], \quad (2)$$

$$J_i^{in} = \left[J_{i-1}^{in} + \frac{\eta_{i-1}^{in}}{Bb_{i-1}} A_{i-1,i}^{in} \right] \left[1 - \frac{\gamma_{i-1}^{in}}{b_{i-1}} (a_i - a_{i-1}) \right], \quad (3)$$

where η^{el} , η^{in} , γ^{el} , and γ^{in} are geometry dependent factors

$$\eta_i^{el} = 1.5 + 2.02 \left(\frac{b_i}{W} \right), \eta_i^{in} = 2 + 0.522 \left(\frac{b_i}{W} \right), \quad (4)$$

$$\gamma_i^{el} = 0.5 + 2.92 \left(\frac{b_i}{W} \right), \gamma_i^{in} = 1 + 0.76 \left(\frac{b_i}{W} \right). \quad (5)$$

where b_i is the length of the unbroken ligament. $A_{i-1,i}^{el}$ and $A_{i-1,i}^{in}$ are the increments of the elastic and inelastic area under the load–displacement curve from step $i - 1$ to i , respectively

$$A_{i-1,i}^{el} = \frac{1}{2} (P_i + P_{i-1}) (\delta_i^{el} - \delta_{i-1}^{el}), \quad (6)$$

$$A_{i-1,i}^{in} = \frac{1}{2} (P_i + P_{i-1}) (\delta_i^{in} - \delta_{i-1}^{in}), \quad (7)$$

where P is the load, δ^{el} and δ^{in} are elastic and inelastic components of the displacement, respectively

$$\delta_i^{el} = P_i C_i, \delta_i^{in} = \delta_i - \delta_i^{el}, \quad (8)$$

where C_i is the elastic compliance measured from the i th unloading sequence.

Calculation of Crack Extension

Crack extension is calculated as

$$\Delta a = a_i - a_0, \quad (9)$$

where a_0 is the initial crack size and a_i is the current crack size corresponding to the i th unloading/reloading sequence and can be calculated using the elastic compliance method as

$$\frac{a_i}{W} = 1.000196 - 4.06319u + 11.242u^2 - 106.043u^3 + 464.335u^4 - 650.677u^5, \quad (10)$$

where

$$u = \frac{1}{(\sqrt{BEC_i} + 1)}. \quad (11)$$

The Young's modulus (E) is different for austenite, self-accommodated and reoriented martensite, and it should be selected according to the phase at the nominal testing temperature at which the experiments are performed.

References

- Lagoudas DC (2008) Shape memory alloys: modeling and engineering applications. Springer, Boston
- Otsuka K, Wayman CM (1999) Shape memory materials. Cambridge University Press, Cambridge
- Elahinia MH, Hashemi M, Tabesh M, Bhaduri SB (2012) Manufacturing and processing of NiTi implants: a review. *Prog Mater Sci* 57(5):911–946
- Nematollahi M, Baghbaderani KS, Amerinatanz A, Zamanian H, Elahinia M (2019) Application of NiTi in assistive and rehabilitation devices: a review. *Bioengineering* 6(2):37
- Hartl DJ, Lagoudas DC (2007) Aerospace applications of shape memory alloys. *Proc Inst Mech Eng G* 221(4):535–552
- Benafan O, Brown J, Calkins F, Kumar P, Stebner A, Turner T, Vaidyanathan R, Webster J, Young M (2014) Shape memory alloy actuator design: CASMART collaborative best practices and case studies. *Int J Mech Mater Des* 10(1):1–42
- Karakalas AA, Machairas TT, Saravanos DA (2019) Effect of shape memory alloys partial transformation on the response of morphing structures encompassing shape memory alloy wire actuators. *J Intell Mater Syst Struct* 30(11):1682–1698
- Jape S, Young B, Haghgouyan B, Hayrettin C, Baxevanis T, Lagoudas D, Karaman I (2020) Actuation-induced stable crack growth in near-equiatomic nickel-titanium shape memory alloys: experimental and numerical analysis. *Int J Solids Struct*. <https://doi.org/10.1016/j.ijsolstr.2020.09.032>
- Baxevanis T, Lagoudas D (2015) Fracture mechanics of shape memory alloys: review and perspectives. *Int J Fract* 191(1–2):191–213
- ASTM-E3098 (2017) Standard test method for mechanical uniaxial pre-strain and thermal free recovery of shape memory alloys. ASTM International, West Conshohocken, PA
- E3097, A (2017) Standard test method for mechanical uniaxial constant force thermal cycling of shape memory alloys. ASTM International, West Conshohocken, PA
- Holtz R, Sadananda K, Imam M (1999) Fatigue thresholds of Ni-Ti alloy near the shape memory transition temperature. *Int J Fatigue* 21:S137–S145
- Robertson SW, Ritchie RO (2007) In vitro fatigue–crack growth and fracture toughness behavior of thin-walled superelastic Nitinol tube for endovascular stents: a basis for defining the effect of crack-like defects. *Biomaterials* 28(4):700–709
- Daly S, Miller A, Ravichandran G, Bhattacharya K (2007) An experimental investigation of crack initiation in thin sheets of nitinol. *Acta Mater* 55(18):6322–6330
- Gollerthan S, Herberg D, Baruj A, Eggeler G (2008) Compact tension testing of martensitic/pseudoplastic NiTi shape memory alloys. *Mater Sci Eng, A* 481:156–159
- Gollerthan S, Young M, Baruj A, Frenzel J, Schmahl WW, Eggeler G (2009) Fracture mechanics and microstructure in NiTi shape memory alloys. *Acta Mater* 57(4):1015–1025
- Haghgouyan B, Shafaghi N, Aydiner CC, Anlas G (2016) Experimental and computational investigation of the effect of phase transformation on fracture parameters of an SMA. *Smart Mater Struct* 25(7):075010
- Katanchi B, Choupani N, Khalil-Allafi J, Tavangar R, Baghani M (2018) Mixed-mode fracture of a superelastic NiTi alloy: experimental and numerical investigations. *Eng Fract Mech* 190:273–287
- Maletta C, Sgambitterra E, Niccoli F (2016) Temperature dependent fracture properties of shape memory alloys: novel findings and a comprehensive model. *Sci Rep* 6(1):1–11
- Mutlu F, Anlas G, Moumni Z (2020) Effect of loading rate on fracture mechanics of NiTi SMA. *Int J Fract* 224:151–165
- Maletta C, Sgambitterra E, Furguiele F (2013) Crack tip stress distribution and stress intensity factor in shape memory alloys. *Fatigue Fract Eng Mater Struct* 36(9):903–912
- Ahadi A, Sun Q (2016) Grain size dependence of fracture toughness and crack-growth resistance of superelastic NiTi. *Scripta Mater* 113:171–175
- ASTM-E399 (2020) Standard test method for linear-elastic plane-strain fracture toughness of metallic materials ASTM international. West Conshohocken, PA
- Robertson S, Pelton A, Ritchie R (2012) Mechanical fatigue and fracture of Nitinol. *Int Mater Rev* 57(1):1–37
- Haghgouyan B, Hayrettin C, Baxevanis T, Karaman I, Lagoudas DC (2019) Fracture toughness of NiTi-towards establishing standard test methods for phase transforming materials. *Acta Mater* 162:226–238
- Rice JR (1968) A path independent integral and the approximate analysis of strain concentration by notches and cracks. *J Appl Mech* 35(2):379–386
- ASTM-E1820 (2020) Standard test method for measurement of fracture toughness. ASTM International, West Conshohocken, PA
- Anderson TL (2017) Fracture mechanics: fundamentals and applications. CRC Press, Boca Raton
- Spinner S, Rozner A (1966) Elastic properties of NiTi as a function of temperature. *J Acoust Soc Am* 40(5):1009–1015
- Dunand DC, Mari D, Bourke M, Roberts J (1996) NiTi and NiTi-TiC composites: part IV Neutron diffraction study of twinning and shape-memory recovery. *Metall Mater Trans A* 27(9):2820–2836
- Rajagopalan S, Little A, Bourke M, Vaidyanathan R (2005) Elastic modulus of shape-memory NiTi from in situ neutron diffraction during macroscopic loading, instrumented indentation, and extensometry. *Appl Phys Lett* 86(8):081901
- Calkins FT, Mabe JH (2010) Shape memory alloy based morphing aerostructures. *J Mech Des* 132(11):111012

33. Benafan O, Moholt M, Bass M, Mabe J, Nicholson D, Calkins F (2019) Recent advancements in rotary shape memory alloy actuators for aeronautics. *Shape Mem Superelast* 5(4):415–428
34. Mohajeri M, Case R, Haghgouyan B, Lagoudas DC, Castaneda H (2020) Loading influence on the corrosion assessment during stress-induced martensite reorientation in nickel-titanium SMA. *Smart Mater Struct* 29(3):035013
35. Jiang D, Kyriakides S, Landis CM (2017) Propagation of phase transformation fronts in pseudoelastic NiTi tubes under uniaxial tension. *Extreme Mech Lett* 15:113–121
36. Chemisky Y, Meraghni F, Bourgeois N, Cornell S, Echchorfi R, Patoor E (2015) Analysis of the deformation paths and thermo-mechanical parameter identification of a shape memory alloy using digital image correlation over heterogeneous tests. *Int J Mech Sci* 96:13–24
37. Sidharth R, Wu Y, Brenne F, Abuzaid W, Sehitoglu H (2020) Relationship between functional fatigue and structural fatigue of iron-based shape memory alloy FeMnNiAl. *Shape Mem Superelast* 6:256
38. Sgambitterra E, Maletta C, Furguele F (2015) Investigation on crack tip transformation in NiTi alloys: effect of the temperature. *Shape Mem Superelast* 1(2):275–283
39. Haghgouyan B, Jape S, Baxevanis T, Karaman I, Lagoudas DC (2019) Stable crack growth in NiTi shape memory alloys: 3D finite element modeling and experimental validation. *Smart Mater Struct* 28(6):064001
40. Young B, Haghgouyan B, Lagoudas D, Karaman I (2019) Effect of temperature on the fracture toughness of a NiTiHf high temperature shape memory alloy. *Shape Memory Superelast* 5(4):362–373
41. Baxevanis T, Landis CM, Lagoudas DCJAM (2014) On the fracture toughness of pseudoelastic shape memory alloys. *J Appl Mech Trans ASME* 81(4):041005
42. Baxevanis T, Chemisky Y, Lagoudas D (2012) Finite element analysis of the plane strain crack-tip mechanical fields in pseudoelastic shape memory alloys. *Smart Mater Struct* 21(9):094012

Publisher's Note Springer Nature remains neutral with regard to jurisdictional claims in published maps and institutional affiliations.